Ab initio determination of the crystal structure of cytochrome c_6 and comparison with plastocyanin

C Frazão[1], CM Soares[1], MA Carrondo[1,2], E Pohl[3], Z Dauter[4], KS Wilson[4], M Hervás[5], JA Navarro[5], MA De la Rosa[5] and GM Sheldrick[3]*

[1]Instituto de Tecnologia Química e Biológica and [2]Instituto Superior Técnico, Apartado 127, 2780 Oeiras, Portugal, [3]Institut für Anorganische Chemie der Universität Göttingen, Tammannstraße 4, 37077 Göttingen, Germany, [4]European Molecular Biology Laboratory, c/o DESY, Notkestrasse 85, 22603 Hamburg, Germany and [5]Instituto de Bioquímica Vegetal y Fotosíntesis, Universidad de Sevilla Y CSIC, Apartado 1113, 41080 Sevilla, Spain

Background: Electron transfer between cytochrome *f* and photosystem I (PSI) can be accomplished by the heme-containing protein cytochrome c_6 or by the copper-containing protein plastocyanin. Higher plants use plastocyanin as the only electron donor to PSI, whereas most green algae and cyanobacteria can use either, with similar kinetics, depending on the copper concentration in the culture medium.

Results: We report here the determination of the structure of cytochrome c_6 from the green alga *Monoraphidium braunii*. Synchrotron X-ray data with an effective resolution of 1.2 Å and the presence of one iron and three sulfur atoms enabled, possibly for the first time, the determination of an unknown protein structure by *ab initio* methods. Anisotropic refinement was accompanied by a decrease in the 'free' R value of over 7%; the anisotropic motion is concentrated at the termini and between residues 38 and 53. The heme geometry is in very good agreement with a new set of heme distances derived from the structures of small molecules. This is probably the most precise structure of a heme protein to date.

Conclusions: On the basis of this cytochrome c_6 structure, we have calculated potential electron transfer pathways and made comparisons with similar analyses for plastocyanin. Electron transfer between the copper redox center of plastocyanin to PSI and from cytochrome *f* is believed to involve two sites on the protein. In contrast, cytochrome c_6 may well use just one electron transfer site, close to the heme unit, in its corresponding reactions with the same two redox partners.

Structure 15 November 1995, **3**:1159–1169

Key words: *ab initio* structure solution, anisotropic refinement, crystal structure, cytochrome, electron transfer

Introduction

Cytochrome c_6 is a 89 amino acid heme-containing redox protein the physiological function of which is the transfer of electrons from the cytochrome b_6f complex to the chlorophyll molecule P700 in photosystem I (PSI) during oxygenic photosynthesis. Cytochrome c_6 is the only electron donor to PSI in some cyanobacterial species, but it has been replaced by the copper-containing protein, plastocyanin, in higher plants; however, other cyanobacterial and algal species can synthesize either cytochrome c_6 or plastocyanin [1–3]. The production of one or the other protein depends mainly on the concentration of copper in the culture medium. If this is too low, then cytochrome c_6 is synthesized instead of plastocyanin. The equivalent physiological role of these two proteins is reflected by their similar sizes and redox potentials. The two metalloproteins are acidic in green algae, as is plastocyanin in higher plants, but both can be either acidic, neutral or basic in cyanobacteria. The probable mechanism (and kinetic efficiency) of the reaction of both proteins with PSI differs from one organism to another, but is almost identical for both within the same organism, indicative of convergent evolution of the two proteins in each organism [4]. Campos *et al.* [5] reported that cytochrome c_6 from the green alga *Monoraphidium braunii* exhibits unusual electron paramagnetic resonance and Mössbauer spectra, which led to the proposal of two forms, I and II, with different crystal field parameters. We have recently reported the crystallization and preliminary diffraction studies of *M. braunii* cytochrome c_6 [6].

Protein crystal structures are usually solved by multiple isomorphous replacement (MIR) methods, which involve the time- and protein-consuming preparation of heavy-atom derivatives, or by molecular replacement, which requires significant structural similarity to a previously determined structure. In contrast, the crystal structures of small molecules, comprising up to about 200 unique atoms, are routinely solved by highly automated and objective direct methods programs. Indeed, for practical purposes, the crystallographic phase problem has been solved for small molecules. For the 9.3 kDa cytochrome c_6 protein, the availability of data to atomic resolution plus the presence of one iron and three sulfur atoms enabled us to solve the structure by methods similar use the single wavelength native data alone, without the need for heavy-atom derivatives, anomalous dispersion, or a related structure as a search fragment. The low sequence identity of cytochrome c_6 (<24%) with known structures would make it difficult to solve this structure by molecular replacement. The recent solution of two cytochrome c' structures by a combination of molecular

*Corresponding author.

 ISSN 0969-2126

replacement, anomalous scattering, and a great deal of skill [7] illustrates the potential difficulties in solving structures of this type by established methods.

Extensive tests [8,9] on the known structures of the small proteins rubredoxin and crambin had convinced us that it should be possible to solve protein crystal structures by *ab initio* methods, provided that a few heavier atoms such as iron or even sulfur are present, and provided that X-ray data can be obtained to atomic resolution (1.2 Å or better). This approach involves the location of the iron and sulfur atoms by computer interpretation of the super-sharpened Patterson vector superposition minimum function [8], followed by automatic iterative expansion to the full structure [9], without the need for interactive graphics etc. Cytochrome c_6 fulfilled all the requirements for this approach to be successful.

Results and discussion

Structure solution

The superposition approach using super-sharp Patterson maps (Fig. 1) with the preliminary 1.3 Å data was indeed able to locate plausible positions for the iron and three sulfurs, and the iron (but not the sulfur) positions could be confirmed from the anomalous ΔF Patterson. Cytochrome c_6 is about twice as large as rubredoxin (used to test the method [8,9]), so the iron and three sulfur atoms constitute a smaller percentage of the total scattering, but the space group (R3 rather than $P2_1$) is less likely to lead to pseudo-centrosymmetric false solutions.

The algorithm [9] for generating the full structure from such a small fragment (in this case Fe+3S) is based on the method employed in the widely distributed small-molecule structure solution program SHELXS-86 [10]. In this program, the algorithm is used to clean up the relatively noisy maps from the direct methods phasing. This peak list optimization algorithm is completely automatic and is based entirely on the peaks of a Fourier map; the only use of chemical information is that the given cell contents are used to assign element types (in order of peak height), and that peaks too close to one of the starting atoms or to higher peaks are eliminated. The peak list is scanned twice, starting with the weakest peak. If removal of an atom increases the correlation coefficient [11] between E_o and E_c (where E_o is the observed X-ray structure factor F_o after normalizing to remove the effects of thermal motion and the electron distribution, and E_c is the corresponding calculated value [using suitably normalized scattering factors]) the atom is deleted, otherwise it is retained. The remaining atoms (including the 'heavier' atoms) are then used to calculate phases for a new E-Fourier, and this peak list optimization is repeated several times. Sim weights [12] are used for all maps. Sim-weighted E-Fouriers at intermediate resolution look quite different from typical protein maps — they are extremely sharp, but noisy. Connectivity, the most sought-after feature in protein electron-density maps, is conspicuous by its absence. When the resolution of the data is insufficient, the percentage of correct peaks becomes too low for interpretation, although some atoms are still accurately placed.

With the full data collected to 1.1 Å, the peak list optimization proceeded smoothly, and it proved possible to build up the structure in stages, adding only those peaks that made chemical sense, then repeating the peak list optimization. The E-maps before and after the first iteration are shown in Figure 2. The atoms were identified and labeled individually by standard small-molecule methods without the interactive interpretation of electron-density maps. In some cases, obvious missing atoms were generated by interpolation. About 85% of the protein atoms could be placed correctly by this purely small-molecule method. It then proved necessary to examine F_o–F_c and $2F_o$–F_c maps with interactive computer graphics [13] to complete the structure. In particular, two regions with high apparent thermal motion, the N-terminal five residues and residues 40–45, could not be interpreted correctly on the basis of the peak lists alone. The peak list optimization was not successful using the preliminary 1.3 Å data and the same iron and sulfur positions.

Because the usual protein crystallographic practice is to work from lower to higher resolution, a comment on the role of the high-resolution data is required. Although the ratio of the iron to carbon scattering factors (Fig. 3)

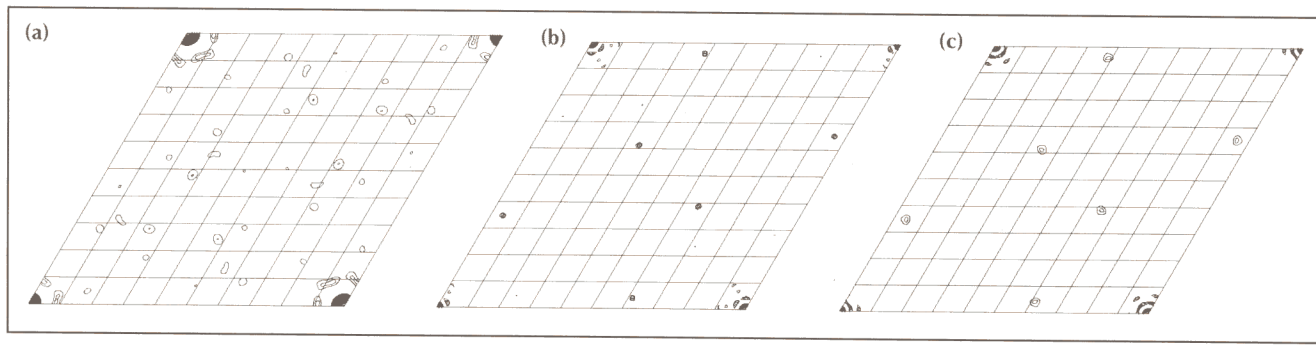

Fig. 1. The Harker section (z=0 for hexagonal axes) of **(a)** the conventional F^2-Patterson function, **(b)** the super-sharp Patterson function calculated with coefficients $(E^3F)^{1/2}$ and **(c)** the anomalous $(\Delta F)^2$-Patterson function. All three maps were calculated from the initial 1.3 Å synchrotron data (wavelength 0.80 Å). Whereas (b) and (c) both immediately reveal the position of the iron atom, the conventional Patterson function (a) is uninformative.

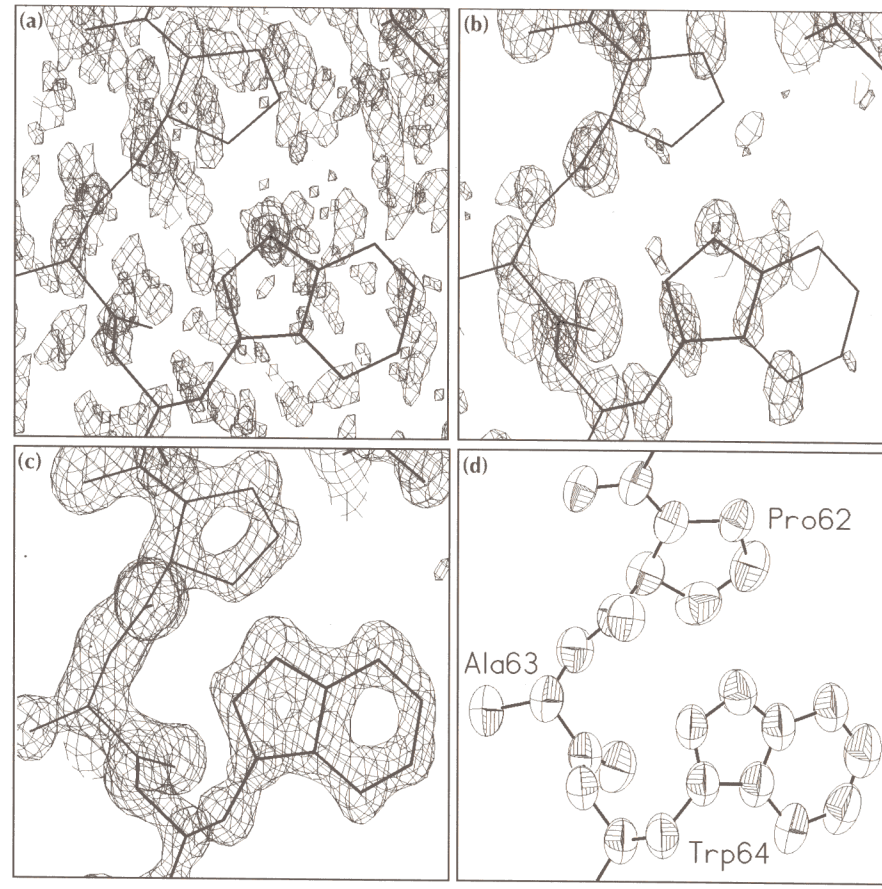

Fig. 2. Residues 62–64 in the course of structure determination. All maps were calculated using the full 1.1 Å data and the program O [13]. **(a)** Sim-weighted E-map with phases from the iron and three sulfur atoms. This map contains some correct resolved peaks and a great deal of noise. **(b)** E-map after peak list optimization [9] starting from (a). Many of the peaks correspond to correct atoms, but the atoms with higher B values (e.g. at the end of side chains) tend to be missing. Iterative application of this small-molecule procedure without the use of interactive computer graphics led to the correct location of ~85% of the protein atoms. **(c)** The final $3F_o–2F_c$ map for the same region. This structure is clearly close to the crucial atomic resolution limit. **(d)** Probability ellipsoids (20%) after anisotropic refinement. The anisotropy is more pronounced for the atoms at the end of side chains, for some of the proline ring atoms (envelope flip), and for the carbonyl oxygens, which tend to move at right angles to the C=O bonds.

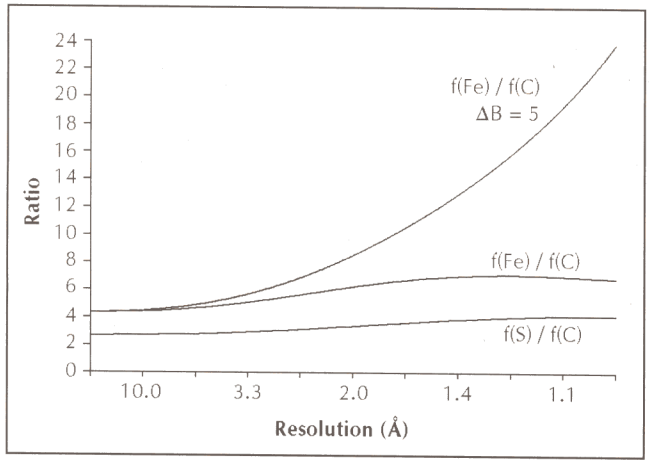

Fig. 3. The relative scattering factors f(Fe)/f(C) and f(S)/f(C) are shown as a function of the resolution d. Although the ratio of the iron to carbon scattering factors increases from 4.3 to about 7 in the resolution range corresponding to the data as a result of the inner core electrons, it will be seen that if the difference in apparent thermal motion (B values) is also taken into account, the ratio becomes very much larger at very high resolution.

increases from 4.3 at infinite resolution to about 7 at 1.3 Å resolution, this is scarcely enough to explain the successful location of the iron and sulfur atoms using the super-sharp Patterson function or the ability to phase the rest of the structure from such a small part of the total scattering power. For the refined structure the following mean B values (equivalent isotropic displacement parameters) were observed: Fe, 11.4 Å^2; S, 13.2 Å^2; heme (except side chains), 12.2 Å^2; main chain, 20.8 Å^2; side chain, 25.4 Å^2 and water, 39.2 Å^2. Taking the differences in B values into account, the ratio in scattering factor between the iron atom and a carbon atom at 1.3 Å resolution is not 7 but 28 (for main-chain carbon atoms) and 56 (for side-chain carbon atoms). Thus, the use of very high-resolution data enables the structure solution to be broken down into several stages; the atoms were indeed located iteratively in the order: Fe+3S; heme; main-chain atoms; side-chain atoms and water molecules. In the critical initial stages, the effective number of atoms is substantially reduced, that is, the protein has almost been turned into a small molecule. At a more normal protein limiting resolution of (say) 2.3 Å, the iron and sulfur atoms would be much less dominant.

Structure refinement

The structure was refined with the program SHELXL [14] using the full resolution range, without the need for a preliminary molecular dynamics stage. Except for the heme group, standard restraints were applied to the geometrical [15] and isotropic or anisotropic displacement parameters [14]. Tables 1 and 2 show the course of the refinement. A dramatic drop of over 7% occurs in R and R_{free} [16,17] on making the structure anisotropic. Restrained anisotropic motion appears to be a rather good description of the dynamical behavior of this protein. The modeling of 12 disordered side chains (including disordered main-chain atoms for the two

Table 1. Cytochrome c_6 refinement progress.

	Water	Parm.	Restr.	R	R_{free}	R(4σ)	R_{free}(4σ)
Iso., no disorder	25	2910	2912	26.8	28.5	24.4	25.9
Anisotropic	25	6545	8364	18.5	20.8	16.6	18.6
Disorder+water	62	7300	9495	16.6	20.3	14.6	18.1
More water	86	7643	9772	15.6	19.8	13.6	17.7
More water	107	7877	9994	15.2	19.9	13.2	17.7
H-atoms	107	7877	9992	14.6	19.1	12.6	17.0
More water	124	8009	10158	14.3	19.0	12.3	16.9
Half-occ.	92+59/2	8217	10263	13.9	18.8	11.9	16.7

$R=\Sigma|F_o-F_c|/\Sigma F_o$, expressed as a percentage. Water, number of water molecules; Parm., number of parameters refined; Restr., number of restraints. The entries in the first column indicate the new features added in the corresponding refinements: iso, isotropic; half-occ., refinement with some of the water occupancies fixed at one-half, and the rest at one.

Table 2. Final refinement (against F^2 for all unique data).

Number of residues	89+heme
Number of discretely disordered residues	12
Rmsd from ideal bond distances	0.013 Å
Rmsd from ideal angle distances	0.032 Å
Rmsd from restraint planes (side chains)	0.016 Å
Rmsd rigid bond $\lvert u_A^2-u_B^2 \rvert$	0.005 Å^2

R=14.0 (32653 data), R(4σ)=12.0 (24579 data).

amino acids at the N terminus) and the improvements to the solvent model produced further, albeit more modest, reductions in R_{free}. It would have been possible to reduce the conventional R factor further by adding more (partially occupied) waters, but the minimum in R_{free} (18.8%; Table 1) was achieved with a model containing 92 fully occupied and 59 half-occupied waters.

Structure description

The *M. braunii* cytochrome c_6 secondary structure (see Fig. 4), follows the topology of class I cytochromes *c* [18]. The peptide chain folds into four helices and three loops, involving six reverse turns, wrapping around the heme and leaving the edge of pyrrole ring C and the D propionic group exposed (see Fig. 5 for heme nomenclature). Cytochrome c_6 is topologically more similar to cytochrome *c*551 of *Pseudomonas aeruginosa* than to other class I cytochromes *c* of known structure [18].

The heme plane separates the peptide chain into two regions, here called N and C, and is covalently attached to the polypeptide chain by the two thioether bonds involving Cys15 and Cys18. The octahedral coordination of the iron atom is completed by the axial ligands His19 and Met61. His19 coordinates to the iron through Nε2, while Nδ1 forms a hydrogen bond with the carbonyl oxygen of Gly23. This hydrogen bond is responsible for the orientation of the histidine plane relative to the NB-(Fe)-ND vector, which in this structure is 27°, i.e. this histidine has been rotated 27° about the Nε2–Fe axis from the position that eclipses NB and ND (Fig. 5). In other class I *c*-type cytochromes, the hydrogen bond from the histidine Nδ1 atom usually involves a carbonyl oxygen of a conserved proline. The only other histidine residue, His30, is at the molecular surface, close to the exposed propionate group of the heme; it would require a substantial conformational change for it to replace the methionine in the coordination shell of the iron atom [5].

The first and the last helices, close to both termini, interact in a characteristic arrangement for this class of proteins. The second and the third helices, shorter and not present in all members of the family, reside on opposite sides of the heme plane. The first of the three interconnecting loops contains an omega-shaped section (Gly22–Leu32),

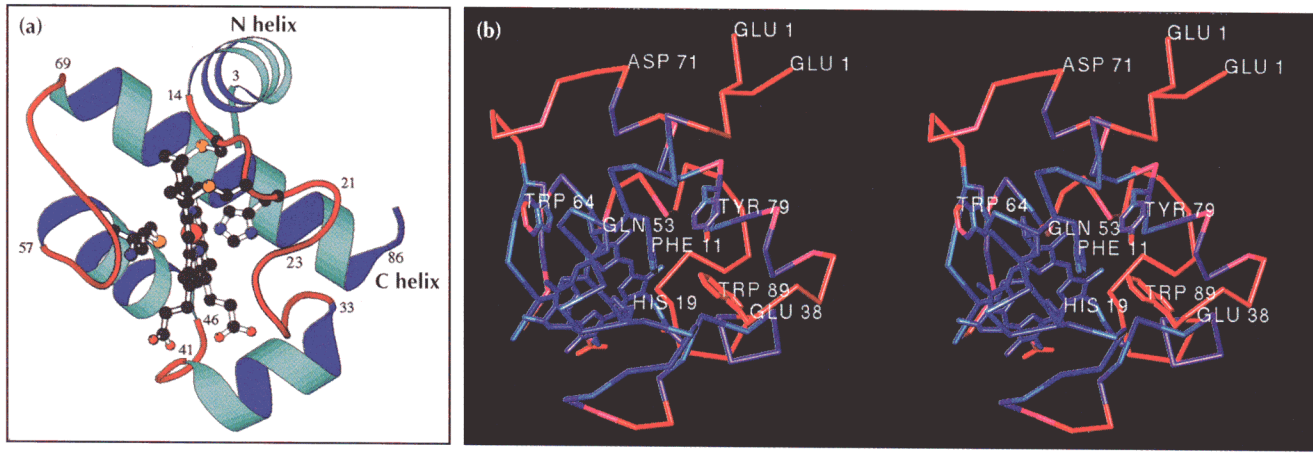

Fig. 4. The cytochrome c_6 secondary structure. **(a)** The heme plane separates the peptide chain into two regions. The N region consists of an initial α helix, residues Asp3–Asn14, followed by the characteristic heme-*c* Cys-X-X-Cys-His binding motif, and three reverse turns within a loop bridging to the second α helix (residues Gln33–Leu41). The C region begins with a reverse turn leading to the third α helix (residues Asn46–Gly57), followed by a loop with two reverse turns and finishing with the final, C helix (residues Asp69–Gly86). (Figure drawn with MOLSCRIPT [44].) **(b)** Stereo Cα trace of another view with some relevant side chains, showing the two alternative conformations of the N terminus and color coded according to temperature factors (blue, 7 Å^2 to red, 23 Å^2). (Figure drawn with TURBO-FRODO [45].)

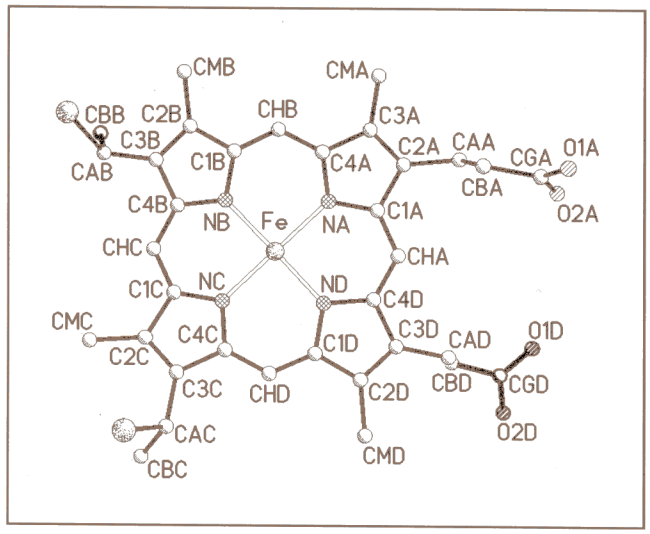

Fig. 5. The atom numbering scheme for the heme group. In cytochromes *c* the heme is covalently bonded to the rest of the protein through two cysteinyl groups (the corresponding sulfur atoms are shown).

which brings additional structural stability to this loop [19]. This is achieved by two main chain to side chain hydrogen bonds from the backbone amide groups of Val26 and Ile27 to Oδ1 of Asn24 (Table 3). This loop contains three reverse turns: one of type II (Ala20-Gly21); another of type I′ (Gly21-Gly22); and the third of type I (Pro28-Asp29). The three consecutive glycines, 21, 22 and 23, are arranged in a 3_{10} helix with unexpectedly low B values (Fig. 4b). This 3_{10}-helical turn is a conserved structural element in cytochromes *c* [18], which explains why Gly22 is absolutely conserved within the c_6 family. At the end of the second helix, the peptide crosses over to the protein C region through a six amino acid loop containing a type II reverse turn (Asp42-Gly43). The anisotropic motion is concentrated in the region between residues 38 and 53, and at the N terminus. It was precisely these regions that proved difficult for the *ab initio* phasing. The structure becomes more rigid again with the third loop, through the sixth covalent ligand to the iron and its invariant neighbors, Met61, Pro62 and Ala63. This section lies between two reverse turns, of types II′ and II, involving Gly59-Ala60 and Asp65-Gly66 respectively, and is further stabilized by five hydrogen bonds (Table 3) and by the hydrophobic interactions in which the Trp64 side chain is involved. In general, the region on the C side of the heme is more labile, with a hot spot in the acidic region Asp69-Glu70-Asp71-Glu72.

Table 3. Hydrogen bonds involved in loops.

Loop	MC–MC	Distance	MC–SC	Distance
15–31	11O...16N	2.96 Å	24Oδ1...26N	2.91 Å
	15O...18N	3.07 Å	24Oδ1...27N	2.96 Å
	18O...25N	2.90 Å	30O...24Nδ2	2.93 Å
	27O...30N	2.96 Å	30Oδ1...6N	3.14 Å
	29O...31N	3.03 Å	31Oγ1...33N	3.22 Å
41–45	37O...41N	2.94 Å		
	41O...44N	2.83 Å		
58–68	54O...64N	2.82 Å	63O...67Nη1	2.97 Å
	55O...65N	3.22 Å		
	58O...61N	2.87 Å		
	61O...58N	3.01 Å		
	64O...67N	2.99 Å		
	64O...68N	3.20 Å		

MC=main chain; SC=side chain.

The heme prosthetic group is located in a hydrophobic pocket, bordered by 23 amino acids, of which 16 have their side chains within 4.0 Å of the heme. Amongst these 23, 13 are either invariant (7) or conservatively replaced (6) in the 21 cytochrome c_6 sequences in the SWISS-PROT database [20], and 12 have hydrophobic characteristics. Four residues are consistently aromatic, namely Phe11, Trp64, Tyr79 and Trp89. Two of them (Phe11 and Trp64) are located near the heme and all four contact the protein surface. Only Phe11 is invariant throughout the available sequences. The first three of these four residues also have relatively low B values and anisotropies, indicating a structural role. Using a rolling probe of radius 1.4 Å (as implemented in X-PLOR [21]), we calculate that 6% of the heme surface is exposed to the solvent, which is close to the 4% average quoted for this family of cytochromes [18]. Atoms CMC and CBC at the edge of ring C, with 9% and 47% of their accessible area exposed to the solvent, and CGD, O1D and O2D from the D propionic group with 12%, 11% and 36% of their solvent-accessible area exposed respectively, allow for direct contact of the heme to a potential electron transfer partner.

The high ratio of acidic (13) to basic (7) surface amino acids is reflected in the macroscopic experimental low isoelectric point of 3.6 found for this cytochrome [5]. Looking in detail at the accessible surface of cytochrome c_6, one acidic negative region can be localized, formed by residues Glu1, Asp69, Glu70, Asp71 and Glu72. Although none of these residues is absolutely conserved, this acidic region is always present in eukaryotic (but not necessarily in prokaryotic) c_6 cytochromes. On the other hand, most of the basic amino acids on the surface are absolutely conserved, but in contrast to the acidic regions, there is no pronounced basic region on the protein surface. Six of the seven basic amino acids (the exception being Arg67) are either neutralized by a salt bridge to an acidic amino acid, or are close to the propionates of the heme.

In the crystal structure, each cytochrome molecule is in contact with eight neighbors in a distorted body-centered cubic arrangement. These contacts use 52% of the solvent-accessible surface area (calculated for an isolated protein molecule). A search for hydrogen bonds (up to a limit of 3.5 Å) showed that there are 15 intermolecular salt bridges, and that 23 water molecules act as bridges between neighboring cytochrome molecules, involving 32 hydrogen bonds.

Geometry of the heme unit

The heme unit is the most rigid part of the structure (Fig. 4b), and can even be refined without geometrical restraints. This structure may well provide the highest resolution data obtained so far for any heme protein, and so creates an opportunity to derive a new set of geometrical restraints for the heme group.

As we were unable to find an up-to-date set of restraint distances for the heme unit based on precise small-molecule structures, we searched the current (April 1995) version of the Cambridge Structural Database (CSD) [22] to find 17 structures, excluding those with high R factors or appreciable disorder, containing suitable heme units. Only structures with hydrogens attached to CHA (and similar atoms) and with aliphatic substituents on C2A and C3A were considered. The presence of a phenyl group on CHA appears to lengthen the C1A–CHA bond significantly. The fourfold or eightfold redundancy of chemically equivalent distances makes this small sample statistically useful. The results of the cytochrome c_6 refinement, in which chemically equivalent distances in the heme core were restrained to be equal to each other (but without the use of target values), are compared with the new CSD values and with frequently used restraint distances (of unknown origin) in Table 4. The agreement is remarkably good, especially between the refinement and the new CSD values (root mean square deviation [rmsd] 0.0046 Å), suggesting that these values would be very suitable as restraints for the refinement of heme structures at lower resolution. Although there will be some under-estimation and fluctuations in the variances caused by the small sample (four or eight), it will be seen that the variances are similar to those of good small-molecule studies.

Table 4. Geometry of the heme group.

Bond	Traditional	This structure	New CSD
NA–C1A	1.384	1.382 (20)	1.381 (18)
C1A–CHA	1.378	1.376 (17)	1.379 (17)
C1A–C2A	1.449	1.445 (23)	1.443 (15)
C2A–C3A	1.334	1.347 (23)	1.355 (19)
NA...C2A	2.312	2.314 (14)	2.318 (14)
NA...CHA	2.450	2.438 (15)	2.442 (16)
C1A...C4D	2.456	2.456 (7)	2.462 (17)
C1A...C4A	2.211	2.203 (14)	2.197 (20)
C1A...C3A	2.247	2.248 (7)	2.248 (16)
C2A...CHA	2.515	2.511 (13)	2.506 (24)

Heme nomenclature is defined in Figure 5. Bond lengths (–) and 1,3-distances (...) are given in Å. The new Cambridge Structural Database (CSD) [22] values are based on an analysis of 17 reliable structures (see text) from the current (April 1995) release. The rmsd is 0.0046 Å between cytochrome c_6 and the new CSD values, and 0.0073 Å between cytochrome c_6 and the traditional values. The estimated standard deviations (esds) in parentheses are the square roots of the variances of the chemically equivalent distances (fourfold or eightfold redundancy per heme unit), in the case of cytochrome c_6 from a refinement in which the corresponding distances were not restrained.

The chiral volumes of the sp^2-hybridized carbon atoms were restrained to be zero, but no other planarity restraints were applied to the heme group, and indeed it is significantly twisted. The iron atom was not restrained in any way; although it lies only 0.008 Å from the mean plane of the heme macrocycle, the rmsd of the heme atoms (ignoring the substituents) is 0.16 Å, and the pyrrole rings are tilted asymmetrically at an average of 7.5° to the mean heme plane. The distortions appear to be caused primarily by the requirements of the covalent cysteine links to the rest of the protein.

Electron transfer pathway

Much of the biochemical interest of cytochrome c_6 lies in the fact that it has been evolutionarily replaced by plastocyanin [2,4,18], with which it shares the properties of very similar kinetic efficiency and redox potential. It is, therefore, natural to expect that the structural characteristics relating to the process of electron transfer will be similar for these two functionally related molecules.

The tertiary structure of plastocyanin is very different from that of cytochrome c_6. It comprises mainly β sheet, with β strands spanning the full length of the molecule. A schematic illustration of plastocyanin from the green alga *Chlamydomonas reinhardtii* (the structure of which has been determined and refined to an R value of 16.8% for data to 1.5 Å resolution by Redinbo *et al.* [23]), is shown in Figure 6. In the following comparisons, the *C. reinhardtii* structure is used because no structural information is available yet for plastocyanin from *M. braunii*. The

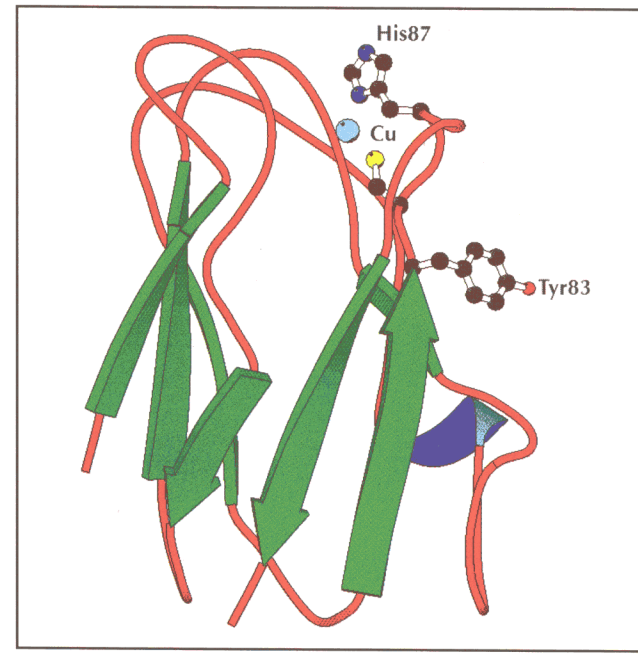

Fig. 6. Schematic representation of plastocyanin from *C. reinhardtii* (PDB entry 2PLT) showing the copper atom (cyan), the side chain of His87, which is believed to constitute one of the possible routes for electron transfer on the hydrophobic northern surface, and the Cys84 and Tyr83 side chains, which constitute the other possible electron transfer route. (Figure drawn with MOLSCRIPT [44].)

redox centers in the two proteins are very different. The cytochrome contains a heme group and plastocyanin has a copper coordinated by two histidines, one methionine and a cysteine. Other structural characteristics of these two proteins have, therefore, to be considered in order to explain their functional similarities.

There has been much speculation on the electron transfer mechanism from cytochrome *f* to plastocyanin, most of it based on experimental evidence [24]. The general view is that the interaction between plastocyanin and cytochrome *f* evolved from a randomly oriented collision mechanism in prokaryotes, to binding by electrostatic complementarity in eukaryotes. Electrostatic complementarity is believed to be achieved by a pair of adjacent negatively charged zones that are conserved in eukaryotes. These zones would interact with complementary positively charged zones on the surface of cytochrome *f*. In Figure 7, the structures of plastocyanin and cytochrome c_6 are shown side by side so that their

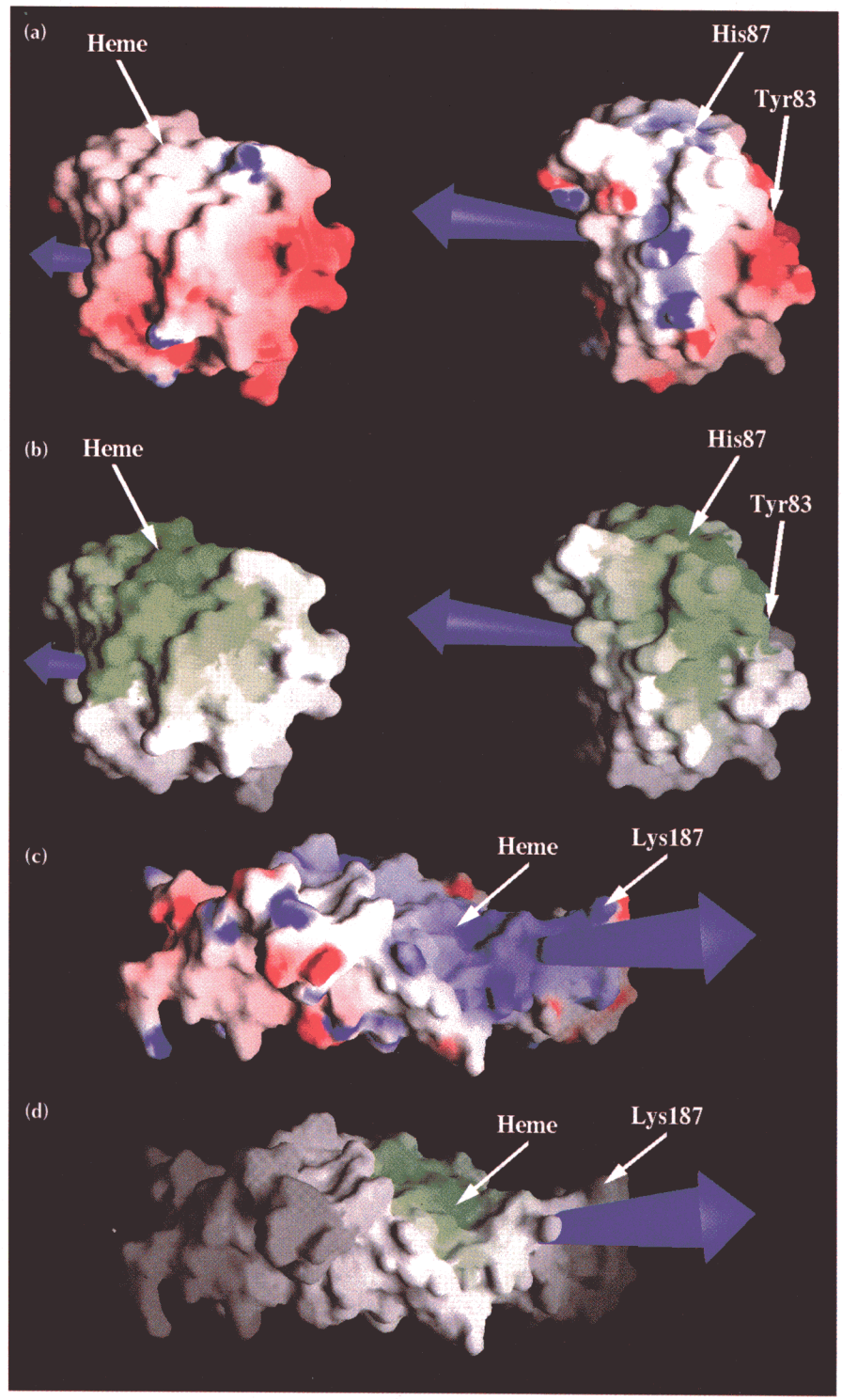

Fig. 7. Electrostatic and electron transfer properties. **(a)** Electrostatic potential mapping at the molecular surface for cytochrome c_6 (left) and plastocyanin (right). The molecules are aligned according to their dipole moments. The molecular dipole moments are shown in blue; the size of the arrow is proportional to the magnitude of the dipole moment. Red zones correspond to negative potentials, while blue zones correspond to positive potentials. The range spans –20 to 10 kT e^{-1}. Both molecules possess a pronounced negative zone corresponding to the negative end of the molecular dipole. **(b)** Electron transfer decay coupling mapping at the molecular surface for cytochrome c_6 (left) and plastocyanin (right). Green zones correspond to high coupling values for electron transfer from the donor center (iron or copper atom) to the surface, while gray zones correspond to low coupling values. The range spans –20 to 0 in $\log_{10}[(\text{decay})^2]$ units as obtained from the program GREENPATH [41]. **(c)** Electrostatic potential and **(d)** electron transfer decay coupling for the molecular surface of cytochrome *f* from *Brassica rapa* (PDB entry 1CMT).

respective molecular dipole moments are in the same direction. These dipole moments provide reference directions for the comparison; they could play a role in the preliminary orientation of the molecules prior to complex formation, but current opinion holds that this is not essential [25]. The main electrostatic features of both proteins are similar (Fig. 7a), although plastocyanin possesses a larger molecular dipole moment. Regions of negative potential predominate at the right hand side of both molecules (Fig. 7a). The negatively charged region of the *M. braunii* cytochrome c_6 includes, amongst others, the Asp69-Glu70-Asp71-Glu72 segment, a region which is consistently acidic in all eukaryotic organisms.

Two potential sites for electron transfer have been suggested for plastocyanin: short-range (His87) and long-range (Tyr83). The latter site is surrounded by the two negatively charged patches mentioned above. This hypothesis is corroborated by electron transfer pathway calculations [26,27]. Experimental evidence suggests that the electron transfer between cytochrome *f* and plastocyanin is mediated by the longer distance pathway, and that electron transfer from plastocyanin to PSI involves the shorter pathway [24].

Details of electron transfer processes are the subject of active research (e.g. see [28]). We have employed the model developed in references [27,29] to compare the electron transfer properties of plastocyanin and cytochrome c_6. Despite its drastic simplifications, this approach has nevertheless given results that were confirmed experimentally [30]. More sophisticated theoretical approaches [31,32] are difficult to apply to such complex systems. The calculations of Betts *et al.* [27] for plastocyanin from *C. reinhardtii* were repeated and the result is depicted in Figure 7b. The short-range site (His87) is an intensive green colour in Figure 7b, indicating that the electron transfer is very favorable from this residue. The long-range site (Tyr83) also has an appreciable calculated coupling value. The same type of calculations were performed for cytochrome c_6 (see Fig. 7b). The zones favorable for electron transfer are clustered around the heme group, far from the negatively charged zone. The favored electron transfer surface is more localized in this molecule than in plastocyanin, probably because of the lack of β sheet motifs, which are efficient at long-distance electron transfer [29,30]. The more probable electron transfer sites at the surface are the solvent-exposed atoms of the heme group itself, namely CMC (with a decay coupling value of –0.89), CBC (–1.33), one of the propionate groups (O1D and O2D, both –2.22), and of residues bonded to the heme, such as the Sγ atom of Cys18 (–1.77). In view of the electron transfer and electrostatic asymmetry, these could constitute a short-range electron transfer site by analogy with plastocyanin. There is no evidence of solvent-exposed residues that could constitute a long-range site in cytochrome c_6.

It is possible that, despite electrostatic similarities, electron transfer mediated by these two different proteins is effected by somewhat different mechanisms. The three-dimensional structure of cytochrome *f* [33] might give some clues about a possible mechanism. Martinez *et al.* [33] looked for conserved positively charged zones among eukaryotic sequences of cytochrome *f* that might act as complementary binding zones for plastocyanin; they located a patch of lysines and arginines in the small domain of the protein that could fulfill this role. Previous studies [34] had shown that one of the residues in this zone, Lys187 (marked in Fig. 7c), could be cross-linked to Asp44 of the negatively charged patch of plastocyanin. Electron transfer pathway calculations were performed for cytochrome *f*, and the results are shown in Figure 7d. The electron transfer zones are located quite far from the positively charged zone, situated mainly around the heme group, which is very exposed in the upper part of the structure. This, in principle, would rule out a long-range electron transfer route, because favorable electrostatic zones are physically separated from potentially favorable electron transfer zones. Thus, a short-range electron transfer site seems more probable.

Martinez *et al.* [33] suggest that, upon binding of plastocyanin, the flexible link between the two domains of cytochrome *f* may permit conformational changes to occur, i.e. the structure that was determined might not be the functional structure with respect to electron transfer. In view of the distance between electrostatically charged and electron transfer zones, this might indeed be a necessity for any type of transfer. Our preliminary studies of docking cytochrome c_6 to cytochrome *f* suggest that the X-ray structure of cytochrome *f* is not adequate for efficient electron transfer. Another possibility to consider is that electron transfer in these systems may be mediated by a short-lived and non-specific interaction, in which only the overall electrostatic characteristics are important, rather than precise docking with multipolar adjustment and exact surface complementarity. Experimental studies of the plastocyanin–cytochrome *f* system have indeed suggested that the electrostatically most stable complex is not optimally oriented for electron transfer [35]. Subsequent rearrangements involving factors other than electrostatics could then guide the complex into a configuration capable of electron transfer.

Biological implications

The heme-containing protein cytochrome c_6 is a soluble electron transport protein involved in oxygenic photosynthesis. In some species of green algae and cyanobacteria, cytochrome c_6 plays the same physiological role (i.e. the transfer of electrons from cytochrome *f* to photosystem I [PSI]) as the copper-containing protein plastocyanin. These organisms synthesize cytochrome c_6 when they are growing in the absence of copper.

A great deal of structural information exists for plastocyanin from higher plants and green algae, but little is known about the structure of its

heme-containing counterpart. This work probably provides the most precise structure determination to date of any heme-containing protein.

It is intriguing to compare the structure of cytochrome c_6 with that of plastocyanin. PSI reduction by plastocyanin or cytochrome c_6 follows an almost identical reaction mechanism when the two proteins are isolated from the same organism, so a degree of structural similarity might have been anticipated. Although the two proteins possess quite different transition metal environments and secondary structural features, there are similarities in terms of their electrostatic properties. The experimental data reported here clearly indicate that the cytochrome c_6 molecule contains not only an acidic region equivalent to the well-known east face of the plastocyanin molecule (with its net protein dipole moment in a similar orientation), but also an electron transfer surface around the heme group that could correspond to the hydrophobic northern surface surrounding His87 of the copper-containing protein. It has been proposed that His87 is involved in the electron transfer pathway from the copper atom in plastocyanin to the photo-oxidized chlorophyll molecule $P700^+$ in PSI. In cytochrome c_6, residues around the heme group, or the heme group itself, could play the same role.

The equivalence between cytochrome c_6 and plastocyanin is, however, barely evident with regard to their putative binding sites for cytochrome *f*. An important difference is that the heme-containing protein lacks an aromatic residue in its acidic patch equivalent to Tyr83 in the copper-containing protein. Tyr83 in plastocyanin does not appear to be involved in electron transfer to P700. However, Tyr83, or another aromatic residue, is probably required for efficient electron transfer from cytochrome *f* to plastocyanin, thereby indicating that electron transfer from cytochrome *f* and to P700 could follow different routes in the plastocyanin molecule. All these findings can be accounted for by assuming that the cytochrome c_6 molecule contains just one site for electron transfer, which is used for interaction with both cytochrome *f* and PSI, whereas plastocyanin reacts with these redox partners via two different routes. Although the model employed here for the electron transfer calculations is primitive and still somewhat speculative, the conclusions are sufficiently decisive that they are unlikely to be affected by reasonable changes in the parameter values, such as the decays associated with the different types of conducting groups.

The structure of cytochrome c_6, determined here by *ab initio* methods similar to those used routinely for solving small-molecule structures, demonstrates the wider applicability of these methods. It also raises hopes of substantial simplification and automation in the process of protein crystal structure determination, at least for metalloproteins that diffract to high resolution.

Materials and methods

Crystal optimization

Media composition for autotrophic growth of *M. braunii* was described by Kessler *et al.* [36]. Experimental conditions for growth and isolation and purification procedures were described by Campos *et al.* [5]. Crystallization searches and the initial crystallization conditions were reported previously [6]. Seeding of new crystals was performed by transferring a droplet containing fragments of an old crushed crystal into a drop containing 1 μl of the precipitating solution (1.5 M sodium citrate and 0.1 M glycine at pH 8.0) and 3 μl of 2.4 mM protein solution in 0.5 mM *N*-tris(hydroxymethyl)methylglycine buffer (pH 7.5). The experiments were carried out on sitting drop bridges from DROP (Devis Precision Outillage Precision, St. Marcellin, France) inside vapor diffusion Linbro (Flow Laboratories, Inc., McLean, VA) plate wells. Usually, too many seeded crystals grew within one day. A droplet containing some of these was sucked up and used for macroseeding under the above conditions; this step was repeated until a reduction to 1–3 crystals per drop was obtained. Crystals showed a trigonal prismatic shape and reached dimensions of 0.8–1.0 mm along all the prism edges, removing the intense red cytochrome color from the solution, which became almost colorless.

Synchrotron diffraction data collection and processing

After initial X-ray investigations using a FAST system [5], synchrotron data for cytochrome c_6 were collected at EMBL, Hamburg, using both original and seeded crystals. For the original crystals, data were collected from 25.0–1.31 Å resolution on the X31 beamline with the EMBL image-plate scanner, using four passes with different crystal to detector distances and exposure times. An incomplete data set for the 2.3–1.2 Å range was collected on the X11 beamline with a MAR image-plate scanner, using original crystals and also a separated crystal satellite, which showed superior diffraction properties. Finally, a data set was collected to 1.1 Å on the BW7B wiggler beamline from seeded crystals using a MAR image-plate scanner. All data processing and merging were performed using the program DENZO [37]. Cell dimensions were a=b=c=40.43 (10) Å (esds in parentheses). Some variation in unit cell dimensions was observed for the different crystals and experimental arrangements; the values used for the refinements are mean values. A total of 274914 data were measured at 20°C from five separate crystals; mean redundancy 8.4, synchrotron wavelength 0.80 Å. In view of the weakness of the data in the outermost resolution shell in Table 5, we consider the effective resolution to be 1.2 Å. In spite of this, the reflections in the 1.2–1.1 Å shell provided useful information in the refinement and especially in the solution of the structure.

Structure refinement

Bond and angle distances were restrained using the target distances from Engh and Huber [15] and esds of 0.02 Å and 0.04 Å respectively, except for the heme core, in which chemically equivalent distances were restrained to be equal but without imposing target values. Chiral volume restraints were applied to the Cα atoms (except glycine) and to the Cβ atoms of threonine and isoleucine; the chiral volumes of the

Table 5. Crystal and reflection data.

Resolution range (Å)	Unique reflec.	Complete (%)	I>2σ (%)	$R_{sym}(I)$*	R†	R(I>2σ)
∞–5.0	354	98.6	98.3	0.03	0.21	0.21
5.0–2.5	2488	99.9	99.0	0.05	0.11	0.11
2.5–1.7	6194	99.9	96.9	0.09	0.10	0.10
1.7–1.4	7107	100.0	89.6	0.15	0.14	0.12
1.4–1.3	4018	100.0	77.6	0.26	0.18	0.14
1.3–1.2	5499	99.9	60.6	0.28	0.26	0.17
1.2–1.1	6993	93.5	39.0	0.52	0.38	0.21
All	32653	98.5	74.1	0.058	0.140	0.120

Space group: R3 (primitive rhombohedral setting). *$R_{sym}(I)=\Sigma|I-\langle I\rangle|/\Sigma\langle I\rangle$, where $\langle I\rangle$ is the mean intensity of a group of equivalent reflections. †$R=\Sigma||F_o|-|F_c||/\Sigma|F_o|$. The percentage of unique reflections measured and the percentage with $I>2\sigma(I)$ are both expressed in terms of the theoretical number of unique reflections.

sp^2-hybridized carbons and proline nitrogens were restrained to be zero, and planarity restraints were applied to the peptide units and aromatic side chains, but not to the heme group. In the anisotropic refinement, rigid-bond restraints were applied to the difference in mean square displacement amplitudes along 1,2-distances and 1,3-distances (esd 0.01 Å^2), and weak similarity restraints (esds 0.05 Å^2 [or 0.1 Å^2 for terminal atoms]) were applied to the corresponding U_{ij} components of atoms within 1.7 Å of each other (including atoms belonging to different components of disordered groups). The solvent water atoms were restrained weakly to be approximately isotropic. No restraints were applied to the iron atom. A diffuse solvent parameter [14] was refined throughout, and anti-bumping restraints [14] were generated automatically.

The data were divided into a working set (90%, 29388 data) and a reference set (10%, 3265 data); the reference set was used only to monitor the refinement using R_{free} [16,17], not for refinement or calculation of maps. All the data were, however, used in the final refinement and maps. Refinement details are presented in Tables 1, 2 and 5. One of the two disorder components of the N terminus gave a point in the 'generously allowed' region of the Ramachandran plot; all other residues were in the core (88%) or allowed (11%) regions according to PROCHECK [38]. The structure was assigned to class I on all the criteria of Morris *et al.* [39]. Atomic coordinates, anisotropic displacement parameters and observed and calculated structure factors have been deposited with the Brookhaven Protein Data Bank for immediate release (entry 1CTJ).

Generation of electrostatic surfaces

Molecular surfaces and electrostatic mapping were generated by the program GRASP [40]. The electrostatic potential was calculated using a simple version of a Poisson–Boltzmann solver, and mapped at the surface by means of a color ramp.

Electron transfer pathways

The calculation of electron transfer coupling values from donor centers was performed using the program GREENPATH [41], which implements semi-empirical methods as developed in references [27,29,42]. These quantify electron transfer pathways (without mutual interference) between a donor and an acceptor in terms of covalent bonds, hydrogen bonds and through-space jumps. Each pathway may involve a combination of several such interactions; the most favorable pathway will be the one with the smallest coupling decay.

GREENPATH [41] allows the calculation of the decay coupling values from a donor group (the copper in plastocyanin and the heme center of the cytochromes) to all the other groups of the protein. For reasons of simplicity, decay couplings are presented as $\log_{10}[(\text{decay})^2]$. This value can be mapped onto the molecular surface (using the value associated with the exposed atoms in the vicinity) using a color ramp. The surface mapping of GREENPATH results was also performed with GRASP [40].

Note added in proof

Since this paper was submitted, the 1.9 Å crystal structure of cytochrome c_6 from *Chlamydomonas reinhardtii* has been published [43].

Acknowledgements: The authors thank A Xavier and M Teixeira for most useful discussions and acknowledge financial support from JNICT (Junta Nacional de Investigação Científica e Tecnológica) (Grant PBIC/C/BIO/1277/92), the Direccíon General de Investigación Cientifica y Técnica (Grants PB90-0099 and PB93-0922), the European Union (Networks CHRX-CT93-0143, CHRX-CT92-0072 and CHRX-CT94-0540, HCMP Large Installations Project CHGE-CT93-0040, and project BIO2-CT94-2052), and the Fonds der Chemischen Industrie. CMS acknowledges a post-doctoral fellowship from PRAXIS XXI (ref. BPD/4151/94). We are grateful to JA Morais and H Terry for assistance with the synchrotron data collection and processing, and to P Lubini and J Wouters for help with the diagrams.

References

1. Bohner, H., Böhme, H. & Böger, P. (1980). Reciprocal formation of plastocyanin and cytochrome c-553 and the influence of cupric ions on photosynthetic electron transport. *Biochim. Biophys. Acta* **592**, 103–112.
2. Sandmann, G., Reck, H., Kessler, E. & Böger, P. (1983). Distribution of plastocyanin and soluble plastidic cytochrome *c* in various classes of algae. *Arch. Microbiol.* **134**, 23–27.
3. Ho, K.K. & Krogmann, D.W. (1984). Electron donors to P700 in cyanobacteria and algae. An instance of unusual genetic variability. *Biochim. Biophys. Acta* **766**, 310–316.
4. Hervás, M., De La Rosa, M.A. & Tollin, G. (1992). A comparative laser-flash absorption spectroscopy study of algal plastocyanin and cytochrome *c*552 photo-oxidation by photosystem I particles from spinach. *Eur. J. Biochem.* **203**, 115–120.
5. Campos, A.P., *et al.*, & Teixeira, M. (1993). Cytochrome c_6 from *Monoraphidium braunii*. A cytochrome with an unusual heme axial coordination. *Eur. J. Biochem.* **216**, 329–341.
6. Frazão, C., *et al.*, & Sheldrick, G.M. (1995). Cytochrome c_6 from the green alga *Monoraphidium braunii*. Crystallization and preliminary diffraction studies. *Acta Cryst. D* **51**, 232–234.
7. Baker, E.N., Anderson, B.F., Dobbs, A.J. & Dodson, E.J. (1995). Use of anomalous scattering with multiple models and data sets to identify and refine a weak molecular replacement solution; structure analysis of cytochrome *c'* from two bacterial species. *Acta Cryst. D* **51**, 282–289.
8. Sheldrick, G.M., Dauter, Z., Wilson, K.S., Hope, H. & Sieker, L.C. (1993). The application of direct methods and Patterson interpretation to high-resolution native protein data. *Acta Cryst. D* **49**, 18–23.
9. Sheldrick, G.M. & Gould, R.O. (1995). Structure solution by iterative peaklist optimization and tangent expansion in space group P1. *Acta Cryst. B* **51**, 423–431.
10. Sheldrick, G.M. (1990). Phase annealing in SHELX-90: direct methods for larger structures. *Acta Cryst. A* **46**, 467–473.
11. Fujinaga, M. & Read, R.J. (1987). Experiences with a new translation-function program. *J. Appl. Cryst.* **20**, 517–521.
12. Sim, G.A. (1959). The distribution of phase angles for structures containing heavy atoms. *Acta Cryst.* **12**, 813–815.
13. Jones, T.A., Zou, J.Y., Cowan, S.W. & Kjeldgaard, M. (1991). Improved methods for building protein models in electron density maps and the location of errors in these models. *Acta Cryst. A* **47**, 110–119.
14. Sheldrick, G.M. & Schneider, T.R. (1995). SHELXL: high-resolution refinement. *Methods Enzymol.*, in press.
15. Engh, R.A. & Huber, R. (1991). Accurate bond and angle parameters for X-ray protein structure refinement. *Acta Cryst. A* **47**, 392–400.

16. Brünger, A.T. (1992). Free R value; a novel statistical quantity for assessing the accuracy of crystal structures. *Nature* **355**, 472–475.
17. Kleywegt, G.J. & Jones, T.A. (1995). Where freedom is given, liberties are taken. *Structure* **3**, 535–540.
18. Pettigrew, G.W. & Moore, G.R. (1990). *Cytochromes* c, *Biological Aspects*. pp. 194–197, Springer-Verlag, Berlin and Heidelberg.
19. Leszczynski, J.F. & Rose, G.D. (1986). Loops in globular proteins: a novel category of secondary structure. *Science* **234**, 849–855.
20. Bairoch, A. & Boeckmann, A. (1992). The SWISS-PROT protein sequence databank. *Nucleic Acids Res.* **20**, 2019–2022.
21. Brünger, A.T., Kuriyan, J. & Karplus, M. (1987). Crystallographic R factor refinement by molecular dynamics. *Science* **255**, 458–460.
22. Allen, F.H., *et al.*, & Watson, D.G. (1991). The development of versions 3 and 4 of the Cambridge structural database system. *J. Chem. Inf. Comp. Sci.* **31**, 187–204.
23. Redinbo, M.R., Cascio, D., Choucais, M.K., Rice, D., Merchant, S. & Yates, T.O. (1993). The 1.5 Å crystal structure of plastocyanin from the green alga *Chlamydomonas reinhardtii*. *Biochemistry* **32**, 10560–10567.
24. Gross, E.L. (1993). Plastocyanin: structure and function. *Photosynth. Res.* **37**, 103–116.
25. Watkins, J.A., Cusanovich, M.A., Meyer, T.E. & Tollin, G. (1994). A "parallel plate" electrostatic model for biomolecular rate constants applied to electron transfer proteins. *Protein Sci.* **3**, 2104–2114.
26. Christensen, H.E.M., Conrad, L.S., Mikkelsen, K.V., Nielsen, M.K. & Ulstrup, J. (1990). Direct and superexchange electron tunneling at the adjacent and remote sites of higher plant plastocyanins. *Inorg. Chem.* **29**, 2808–2816.
27. Betts, J.N., Beratan, D.N. & Onuchic, J.N. (1992). Mapping electron tunneling pathways: an algorithm that finds the "minimum length/maximum coupling" pathway between electron donors and acceptors in proteins. *J. Am. Chem. Soc.* **114**, 4043–4046.
28. Karpishin, T.B., Grinstaff, M.W., Komar-Panicucci, S., McLendon, G. & Gray, H.B. (1994). Electron transfer in cytochrome *c* depends upon the structure of the intervening medium. *Structure* **2**, 415–422.
29. Beratan, D.N., Betts, J.N. & Onuchic, J.N. (1991). Protein electron transfer rates set by the bridging secondary and tertiary structure. *Science* **252**, 1285–1288.
30. Langen, R., Chang, I.-J., Germanas, Y.P., Richards, J.H., Winkler, J.R. & Gray, H.B. (1995). Electron tunneling in proteins. Coupling through a β-strand. *Science* **268**, 1733–1735.
31. Marcus, R.A. & Sutin, N. (1985). Electron transfers in chemistry and biology. *Biochim. Biophys. Acta* **811**, 265–322.
32. Siddarth, P. & Marcus, R.A. (1993). Electron-transfer reactions in proteins: an artificial intelligence approach to electronic coupling. *J. Phys. Chem.* **97**, 2400–2405.
33. Martinez, S.E., Huang, D., Szczepaniak, A., Cramer, W.A. & Smith, J.L. (1994). Crystal structure of chloroplast cytochrome *f* reveals a novel cytochrome fold and unexpected heme ligation. *Structure* **2**, 95–105.
34. Morand, L.Z., Frame, M.K., Colvert, K.K., Johnson, D.A., Krogmann, D.W. & Davis, D.J. (1989). Plastocyanin–cytochrome *f* interaction. *Biochemistry* **28**, 8039–8047.
35. Meyer, T.E., Zhao, Z.G., Cusanovich, M.A. & Tollin, G. (1993). Transient kinetics of electron transfer from a variety of c-type cytochromes to plastocyanin. *Biochemistry* **32**, 4552–4559.
36. Kessler, E., Langner, N., Ludwig, J. & Wiechmann, H. (1963). *Studies on Microalgae and Photosynthetic Bacteria*. pp. 7–20, Japanese Society of Plant Physiology, Tokyo.
37. Otwinowski, Z. (1993). *DENZO: Program for Macromolecular Data Processing*. Yale University, New Haven, CT.
38. Laskowski, R.A., MacArthur, M.W., Moss, D.S. & Thornton, J.M. (1993). PROCHECK: a program to check the stereochemical quality of protein structures. *J. Appl. Cryst.* **26**, 283–291.
39. Morris, A.L., MacArthur, M.W., Hutchinson, E.G. & Thornton, J.M. (1992). Stereochemical quality of protein structure coordinates. *Proteins* **12**, 345–364.
40. Nicholls, A. (1992). *GRASP: Graphical Representation and Analysis of Surface Properties*. Columbia University, New York.
41. Regan, J.J. (1994). *GREENPATH software v0.971*. San Diego, CA.
42. Beratan, D.N., Onuchic, J.N., Winkler, J.R. & Gray, H.B. (1992). Electron-tunneling pathways in proteins. *Science* **258**, 1740–1741.
43. Kerfeld, C.A., Anwar, H.P., Interrante, R., Merchant, S. & Yeates, T.O. (1995). The structure of chloroplast cytochrome c_6 at 1.9 Å resolution: evidence for functional oligomerization. *J. Mol. Biol.* **250**, 627–647.
44. Kraulis, P.J. (1991). MOLSCRIPT: a program to produce both detailed and schematic plots of protein structures. *J. Appl. Cryst.* **24**, 946–950.
45. Roussel, A. & Cambillau, C. (1989). TURBO-FRODO. In *Silicon Graphics Geometry Partner Directory*. pp. 77–78, Silicon Graphics, Mountain View, CA.

Received: **3 Jul 1995**; revisions requested: **25 Jul 1995**; revisions received: **29 Aug 1995**. Accepted: **7 Sep 1995**.